Earthquake Geotechnical Engineering for Protection and Development of Environment and Constructions – Silvestri & Moraci (Eds)
© 2019 Associazione Geotecnica Italiana, Rome, Italy, ISBN 978-0-367-14328-2

Effect of liquefaction on the seismic response of port facilities on reclaimed island: A case study from the 2016 Kumamoto earthquake sequence

B. Ismael, D. Lombardi, S.M. Ahmad & J.A. Mendoza
University of Manchester, Manchester, UK

S. Bhattacharya
University of Surrey, Surrey, UK

N.J. Vimalan
VJ Tech, Reading, UK

ABSTRACT: Following the 2016 Kumamoto earthquake sequence, which struck the island of Kyushu in Japan, a reconnaissance mission was conducted in the region affected by the seismic events by the UK-based Earthquake Engineering Field Investigation Team (EEFIT). The sequence caused widespread liquefaction in the coastal areas of Kumamoto Prefecture, arguably due to the presence of saturated loose sand deposits. One of the most affected areas was Kumamoto port, which was located on an artificial island made of medium-dense deposits of carbonate sand. Representative soil specimens were sampled from the area and subsequently tested in a triaxial apparatus. The experimental results were used to calibrate the parameters required by the Dafalias-Manzari model. The numerical model demonstrated that full liquefaction occurred in a confined zone at a relatively large distance from the existing foundations, which may explain the limited structural damage observed in the region despite the high-intensity shaking and widespread liquefaction.

1 INTRODUCTION

A series of strong earthquakes struck Japan starting on 14th April 2016 with 6.5 Japan local magnitude (6.2 Mw). Before the occurrence of the main shock on 16th April 2016, another foreshock of 6.4 MJ (6 Mw) was recorded by the Japan Meteorological Agency (JMA) on 15th April 2016. The mainshock magnitude was 7.3 Japan local magnitude (7.1 Mw) (Ismael & Lombardi 2018a). The earthquakes caused a significant loss of both people and infrastructures, where the total number of fatalities was 69, and 1,747 were injured. Furthermore, the damage cost was approximately 24-46 billion dollars (Bhattacharya et al. 2018). Both foreshocks were generated from the Hinagu fault located in the south-west region of Japan at approximately 11 km focal depth, while the main shock was initiated from the Futagawa fault, which is not far from the Hinagu fault, at 12 km focal depth. The faults' type is lateral strike-slip generated from superficial focus depth (Goda et al. 2016).

Most of the observed damage in areas stricken by an earthquake can be attributed to liquefaction, especially when the ground is formed from loose or medium-dense sand. In general, liquefaction is known as the transformation from a solid state to a liquid one. From a soil mechanics standpoint, the liquefaction phenomenon represents the conditions in which most of the soil's stiffness and strength are lost via the application of cyclic loading or any rapid loading. In saturated sand, Excess Pore Water Pressure (EPWP) generated during the application of a seismic load causes a decrease in the effective stress, according to the effective stress principle. In the extreme case, the effective stress becomes zero, and the soil grains lose contact

with each other. At this stage, the soil grains float in the pore water without any confinement. Several factors could be correlated to liquefaction vulnerability. One is the ground geology, where previous earthquakes confirm that the majority of the liquefied soil was found to be fine-grained sand and sandy silt (Huang & Jiang 2010). The grain size distribution of the soil deposit is also considered as a boundary to distinguish between liquefiable and non-liquefiable soil, as suggested by Tsuchida (1970). The last author introduced a grain size distribution curve, in which two boundaries are proposed for liquefiable and highly liquefiable soil. Furthermore, liquefaction amenability could be anticipated by other factors such as the shape and hardness of the particles, besides the percentage of fines in the sample (Verdugo 1989). In-situ tests could be used to predict liquefaction vulnerability, such as Standard Penetration Test (SPT), Cone Penetration Test (CPT) and in-situ shear wave velocity, by using empirical equations such as the codes of practice (e.g. Eurocode8 (1998)) and simplified procedures such as the one suggested by Idriss and Boulanger (2008).

Numerical modelling is a versatile tool which has been used recently to estimate liquefaction taking into account several factors which could not be considered in the empirical equations (Ismael & Lombardi 2018b). Several constitutive models are available to predict the soil's vulnerability to liquefaction (e.g. estimating the ratio of the EPWP to the effective overburden stress in a soil deposit (r_u)) besides liquefaction-related deformations. This task could be considered very challenging, as a result of the continuous variation in the soil condition and state during liquefaction, in addition to the irregularity of the load itself (i.e. earthquake motion). OpenSees (Open System for Earthquake Engineering Simulation) software has been used recently by several researchers as a ground response analysis tool. The Dafalias-Manzari model is used in the current study to model the soil behaviour because it is formulated based on the critical state and bounding surface plasticity frameworks which require a unique set of input parameters for a wide range of relative densities and initial stresses. Using the object-oriented software framework OpenSees, a representative borehole for Kumamoto port has been modelled as a soil column to study the site response analysis for the port area. The model parameters are calibrated based on static and cyclic triaxial tests conducted on a representative sample sampled from the port area.

All along the Kumamoto port area, signs of soil liquefaction were reported including sand boils, uplifted manholes and localised lateral spreading. However, the damage was limited and there was no total collapse for any building or infrastructure in spite of the aforementioned liquefaction signs in the area. One purpose of this study is to present liquefaction-induced failure during the Kumamoto earthquake sequence at Kumamoto port. Then, an attempt will be made to explain the reasons behind the minor damage in the port area despite the obvious liquefaction signs.

2 GROUND MOTION

The ground motion characteristics were obtained from KiK-NET and K-NET operated by the National Research Institute for Earth Science and Disaster Resilience in Japan. The maximum ground motion recorded at KMMH16 station located in Mashiki town (32.7967°N, 130.8199°E) for the mainshock is used in the analysis and shown in Figure 1 (a). Then, the response spectral at 5% damping ratio as recommended by most of the current codes such as Eurocode 8 are presented in Figure 1 (b).

3 POST-EARTHQUAKE FIELD SURVEY AT KUMAMOTO PORT

Kumamoto port is located west of Kumamoto city. This port is an artificial island built on the Ariaka Sea. As a consequence of the Kumamoto earthquake, liquefaction signs were observed at the port area including sand boiling, ground fractures, localised ground lateral spreading, differential settlement and tilting of residential houses. Figure 2 shows the typical surface manifestation of soil liquefaction.

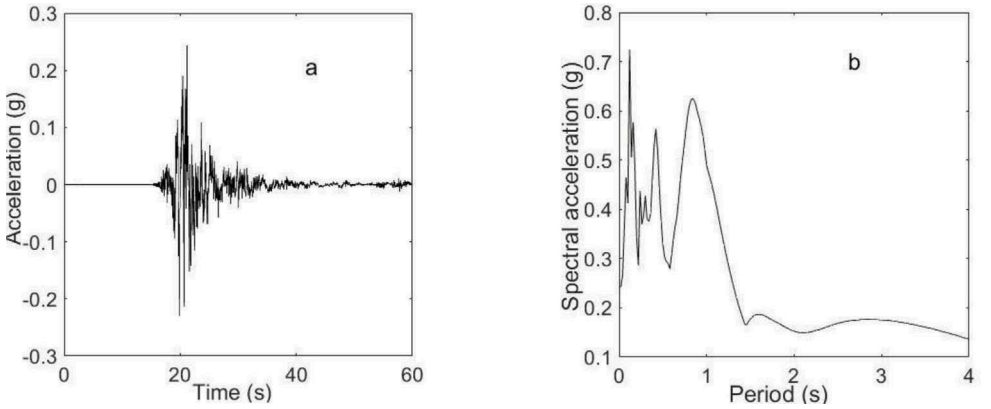

Figure 1. (a) Acceleration time-history for the mainshock at KMMH16 station; (b) Acceleration response spectral.

Figure 2. Typical surface manifestation of soil liquefaction at Kumamoto port.

4 NUMERICAL MODEL FOR LIQUEFACTION PREDICTION

A soil column finite element model is developed to study the site response analysis for the site under investigation. To track the generated EPWP and displacement during the ground shaking, the soil column is modelled using cubic 8-noded BrickUP elements with both displacement and pore water pressure degrees of freedom (Figure 3). Using the aforementioned element type, the interaction between solid soil skeleton and pore fluid could be accounted for, enabling the liquefaction phenomenon to be studied. The nodes above the water table are fixed in the pore pressure DOF to represent the open drainage condition, while the nodes at the base of the soil column are fixed against vertical displacement to account for the bedrock layers that exists below the modelled soil profiles. The dynamic analysis is conducted with the Newmark integrator using the gamma and beta coefficients. According to this method of integration, a combination of $\beta = 0.25$ and $\gamma = 0.5$ is recommended to achieve unconditionally stable analysis.

4.1 *Soil constitutive model*

The Dafalias-Manzari model is constructed based on the dilatancy, bounding and the critical state surfaces. The cyclic and reverse loadings are simulated by postulating the existence of the yield surface in the $q - p'$ space. This elastic region (which is represented geometrically as a wedge) is bounded by the yield surfaces. It is interesting to note that, when q and p' increase at

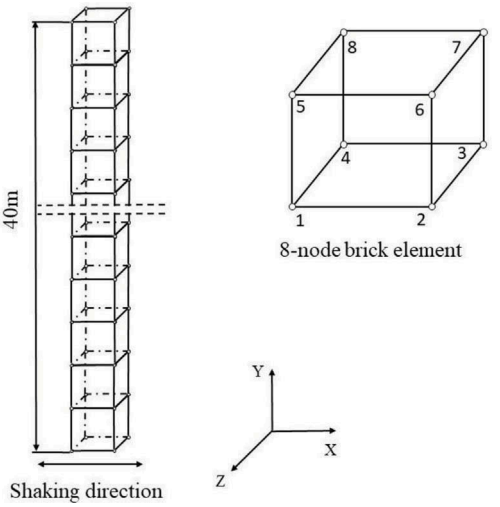

Figure 3. The model of the soil column.

the same stress ratio, η, no plastic deformation will mobilise because the stress path will not tend to cross the wedge zone (Dafalias & Manzari 2004).

4.2 *Calibration of the Dafalias-Manzari model for Kumamoto sand*

The accuracy of numerical modelling depends largely on the parameters selected for a specific model. For that reason, it is necessary to calibrate the material constants by ensuring that those parameters could mimic the stress path as laboratory tests. This could be achieved by using a single element model. Several triaxial tests were conducted on saturated samples sampled from the port area. The experimental programme conducted in this study and the corresponding estimated parameters from each test type are presented in Table 1. The elastic shear modulus of sand, G, is defined using the shear modulus constant G_o. The elastic shear modulus G is dependent on the void ratio (e) and the mean effective stress (p'), according to equation 1, which was introduced by Dafalias and Manzari (2004).

$$G = G_o p_{at} \frac{(2.97 - e)^2}{1 + e} \left(\frac{p'}{p_{at}} \right)^{0.5} \tag{1}$$

Table 1. Testing programme.

Test ID	Test type	Void ratio	Consolidation pressure (kPa)	Parameter
MO-1	Consolidated-drained test	0.99	100	Shear modulus constant
MO-2		0.98	200	G_o
MO-3	Constant mean effective	0.975	100	CSL parameters
MO-4	stress	0.972	200	e_o, λ_c, M
MO-5		0.93	300	
MO-6		0.925	400	
MO-7	Consolidated-undrained	0.97	100	n^b, n^d, A_o, h_0, C_h
MO-8		0.94	200	
MO-9	Cyclic triaxial	1.04	100	C_z, z_{max}

Where p_{at} is the atmospheric pressure for normalisation.

Two monotonic drained triaxial tests were conducted to estimate the shear modulus constant G_o using the deviatoric stress-strain $(q - \mathcal{E}_a)$ at very small strain, as depicted in Figure 4. The critical state line of a soil is defined as the terminal state in which the soil continues to deform at constant values of q, p' and e. In triaxial compression, the ratio of q / p' at critical state is defined by the M parameter, as plotted in Figure 5. During the steady state deformation, the mean effective stress is correlated to the void ratio of a soil. Routinely, many researchers have introduced a linear relation in the e-p' plane. However, recent findings by Li and Wang (1998) suggest the power relation presented in equation 2 below:

$$e_c = e_o - \lambda_c (p_c / p_{at})^{\zeta} \tag{2}$$

Where e_o the void ratio at p_c=0 and λ_c and ζ are constants. An excellent fit of the above equation with data for Kumamoto sand shows that e_o = 1.154, λ_c=0.093 and ζ=0.7, as can be seen in Figure 6. A trial and error procedure was followed to estimate the parameters

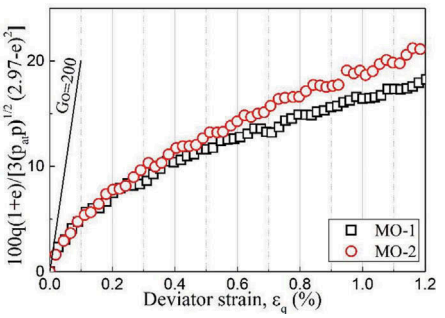

Figure 4. Calibration of the G_o constant using monotonic drained triaxial tests on Kumamoto sand.

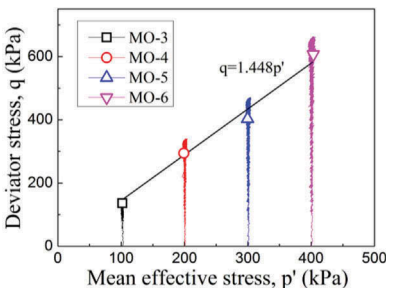

Figure 5. Calibration of the M constant using constant mean effective stress triaxial tests.

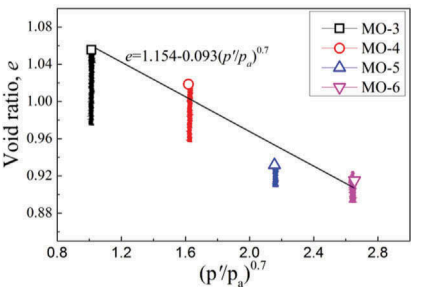

Figure 6. Calibration of the e_o, λc and ζ constants using con-stants mean effective stress triaxial.

Table 2. Material parameters for Kumamoto sand.

Parameter	Variable	Symbol	Kumamoto sand
Elasticity	Shear modulus constant	G_o	200
	Poisson's ratio	ν	0.2
Critical state	Critical state stress ratio	M	1.448
	Ratio of critical state stress ratio in extension and compression	c	0.68
	Critical state line constant	λc	0.093
	Critical void ratio at p = 0	e_o	1.154
	Critical state line constant	ζ	0.7
Yield surface	Yield surface constant (radius of yield surface in stress ratio space)	m	0.02
Plastic modulus	Constant parameter	h_o	8.7
	Constant parameter	C_h	0.91
	Bounding (peak) surface parameter	n^b	1.2
Dilatancy	Dilatancy surface (phase transformation) parameter	n^d	5.2
	Dilatancy parameter	A_o	0.39
Fabric-dilatancy tensor	Constant parameter	C_z	800
	Constant parameter	z_{max}	8

(A_o, n^b, n^d, c_h and h_o). Table 2 presents the calibrated parameters for Kumamoto sand. A comparison of the simulation results with the consolidated undrained cyclic test is presented in Figure 7.

4.3 *Analysis of observed liquefaction at Kumamoto port*

Borehole log, SPT count number and maximum r_u generated at Kumamoto port as calculated by OpenSees software are presented in Figure 8. This figure shows that the full liquefaction (i. e. ru≥0.9) is mobilised in the confined zone between 9 and 22.5 m. Figure 9 shows the seismic response for a representative borehole selected from the port area. As can be seen in this figure, strong evidence of liquefaction is apparent at the site under investigation. The typical mechanism of the decrease in the vertical effective stress occurs as a result of the excess pore pressure generation during the application of the seismic motion. All layers exhibit a reduction in the vertical stresses from the initial values. The signs of the butterfly shape can be observed in the stress path once the vertical effective stress reaches a minimum value. Soon after the shaking starts, the layers that exist at a depth below 9 m start showing full liquefaction and

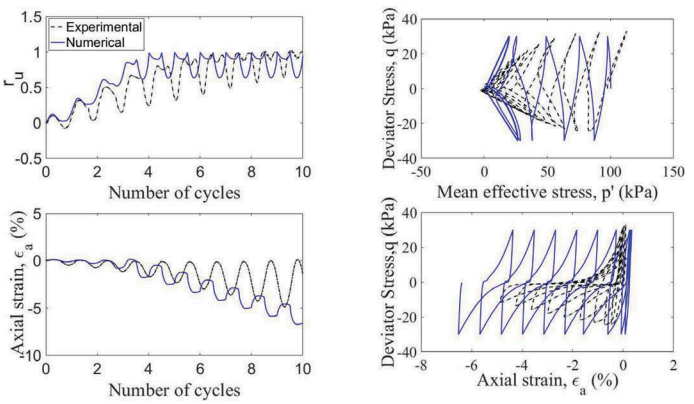

Figure 7. Comparison of simulation results with consolidated undrained cyclic test.

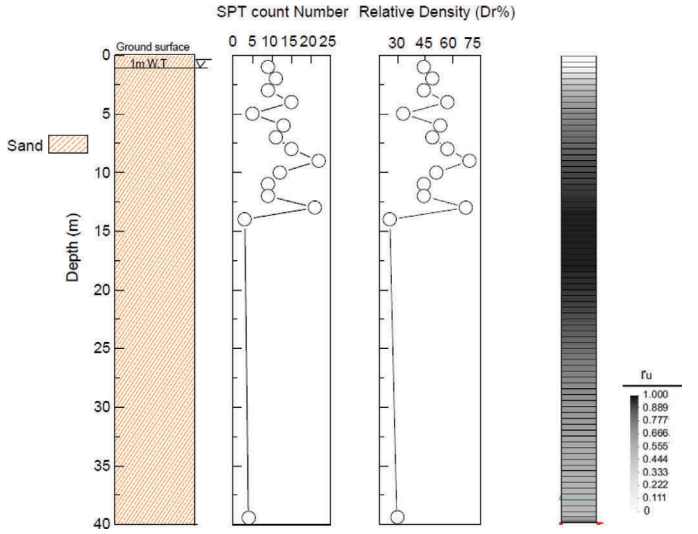

Figure 8. Borehole log, SPT-count profile and maximum r_u generated at Kumamoto port as calculated by OpenSees software.

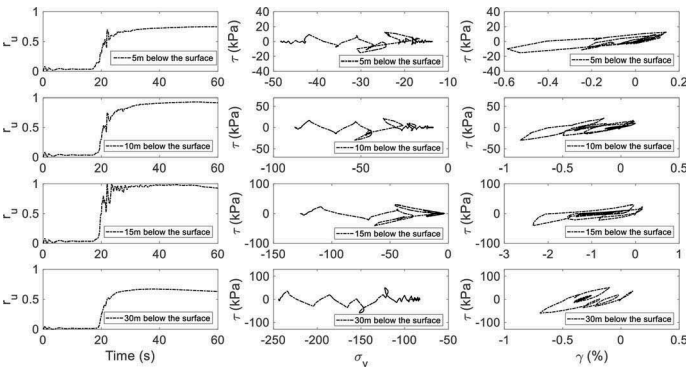

Figure 9. Seismic results for the Kumamoto port soil profile.

the soil remains liquefied well after the end of the shaking (i.e. 30 sec). The stress-strain hysteresis curves show that strains are progressively increasing accompanied by a reduction in the stiffness, confirming the softening behaviour of the liquefied soil. As expected, the maximum shear strain develops at the depth where full liquefaction is anticipated. As a result of this, the soil shows cycles of small shear stress and large shear strain which are correlated to the mobilisation of the pore water pressure with time. This strain-softening response is clear as the slope of the hysteresis curves continues to decrease with the increase of the shear strain, indicating a decrease in the shear modulus of the liquefied soil. When soil liquefies, this progressive decrease in the slope of the stress-strain curve will eventually become a flat curve for fully liquefied soil. However, after a specific strain value, a strain hardening could be observed as the soil regained its stiffness and strength after the liquefaction had occurred.

According to Seed and Lee (1966), liquefaction may develop at any depth within the liquefiable soil (i.e. at the surface or at a depth below the ground surface) if both in-situ conditions and ground motions are sufficient to trigger liquefaction. They also mentioned that the surficial layers may liquefy indirectly, not because of the applied motion but as a consequence of the water flowing in an upward direction, which will induce the conditions required for liquefaction, and/or quicksand in the upper layers.

5 CONCLUSIONS

The lack of structural damage despite the clear surficial liquefaction signs throughout the Kumamoto port (resulting from the presence of saturated sandy soil throughout the area besides the strong recorded ground motion) is a point of particular interest. To study the site response analysis for the Kumamoto port region, a numerical model was built to give further insight into the problem under investigation. The numerical model shows that the soil profile is highly liquefiable with full liquefaction (i.e. ru≥0.9) mobilised in the confined zone between 9 and 22.5 m. The existence of a liquefied layer in a confined zone from both directions (top and bottom) could be correlated to the minor damage in the port area despite the occurrence of liquefaction. The current study confirms that the onset of liquefaction at a large depth from the existing foundations would be of little practical importance.

ACKNOWLEDGEMENTS

The first author would like to acknowledge the technical support received from the Geotechnical labs at Manchester and Surrey universities and VJ Tech for carrying out the soil tests. He would also like to acknowledge the Iraqi Ministry of Higher Education and Scientific Research (MOHESR) for funding his PhD study at the University of Manchester.

REFERENCES

Bhattacharya, S., Hyodo, M., Nikitas, G., Ismael, B., Suzuki, H., Lombardi, D., Egami, S., Watanabe, G. & Goda, K. 2018. Geotechnical and infrastructural damage due to the 2016 Kumamoto earthquake sequence. *Soil Dynamics and Earthquake Engineering*, 104, pp. 390–394. doi: 10.1016/j.soildyn.2017.11.009.

Dafalias, Y. F. & Manzari, M. T. 2004. Simple plasticity sand model accounting for fabric change effects. *Journal of Engineering Mechanics, ASCE*. 130 (6), pp. 622–634.

Eurocode 8. 1998. Design of structures for earthquake resistance part 5: Foundations, retaining structures and geotechnical aspects (English). Brussels: European Committee de Normalisation.

Goda, K., Campbell, G., Hulme, L., Ismael, B., Ke, L., Marsh, R., Sammonds, P., So, E., Okumura, Y., Kishi, N., Koyama, M., Yotsui, S., Kiyono, J., Wu, Sh. & Wilkinson, S. 2016. The 2016 Kumamoto earthquakes: cascading geological hazards and compounding risks. *Frontiers in Built Environment*, 2, pp. 1–23. doi: 10.3389/fbuil.2016.00019.

Huang, Y. & Jiang, X. 2010. Field-observed phenomena of seismic liquefaction and subsidence during the 2008 Wenchuan earthquake in China. *Natural Hazards*, 54(3), pp. 839–850. doi: 10.1007/s11069-010-9509-6.

Idriss, I. & Boulanger, R. W. 2008. *Soil liquefaction during earthquakes*. Oakland, CA: Earthquake Engineering Research Institute.

Ismael, B. & Lombardi, D. 2018a. Evaluation of liquefaction potential for two sites due to the 2016 Kumamoto earthquake sequence. *1st Conference of the Arabian Journal of Geoscience (CAJG)*, 12–15 November, 2018, Hammamet, Tunisia.

Ismael, B. & Lombardi, D. 2018b. Analysis of observed liquefaction during the 2016 Kumamoto earthquake. *Numerical Methods in Geotechnical Engineering IX*. London: Taylor & Francis Group, pp. 837–841.

Li, X. & Wang, Y. 1998. Linear representation of steady-state line for sand. *Journal of Geotechnical and Geoenvironmental Engineering, ASCE*, 124(12), pp. 1215–1217.

Seed, H. B. & Lee, K. L. 1966. Liquefaction of saturated sands during cyclic loading. *Journal of the Soil Mechanics and Foundations* Division, 92(6), pp. 105–134.

Tsuchida, H. 1970. Prediction and countermeasure against the liquefaction in sand deposits. In: Abstract of the seminar in the Port and Harbor Research Institute, 1970. 3.1–3.33.

Verdugo, R. 1989. Effect of fine content on the steady state of deformation on sandy soils. Master's thesis, University of Tokyo.